ACS OMEGA

Open Access

http://pubs.acs.org/journal/acsodf

Article

Bioresorption and Biomineralization of S53P4 Bioactive Glass in Neutral Tris Buffer and Citric Acid Solution

Kwon Jun Yoo,[†] Woo Young Jang,[†] and Jeong Ho Chang*

Cite This: *ACS Omega* 2024, 9, 43678−43688

Read Online

ACCESS | Metrics & More | Article Recommendations

ABSTRACT: In this study, S53P4 ($53SiO_2$−$23Na_2O$−$20CaO$−$4P_2O_5$) bioactive glass (BG) were prepared through a melt-milling process, and their bioresorption and biomineralization behavior was evaluated by in vitro dissolution under different solution conditions (neutral and acidic). The particle size of S53P4 BG was controlled by milling, and the in vitro dissolution evaluation was performed in tris buffer and citric acid solution for 21 days at 37 °C according to ISO 10993-14 (biological evaluation of medical devices). During dissolution, the ion release rate of S53P4 BG was confirmed to be three times faster in citric acid solution than that in tris buffer. Among them, the ion concentration of calcium and phosphorus initially increased and then gradually decreased, which is due to the biomineralization process. This process formed a new layer of particles on the surface of S53P4 BG, which was identified as a calcium-phosphate-based compound by X-ray diffraction analysis. Furthermore, the thickness of the layer was observed to be 273 nm in tris buffer and 34 nm in citric acid solution by focused-ion beam scanning electron microscopy, and the morphology of the particles comprising this layer was observed to be thicker and longer in tris buffer than that in citric acid solution. This difference is due to the citrate present in the citric acid solution interacting with the released calcium ions and inhibiting the formation of a new layer. Thus, the ion release of S53P4 BG was faster in citric acid solution than that in tris buffer, but the biomineralization process to form the calcium phosphate-based compound was more effective in tris buffer.

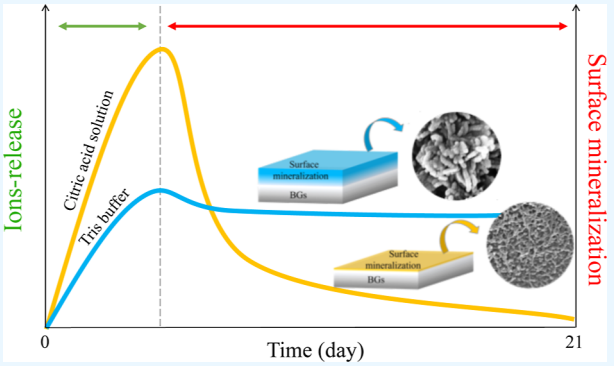

1. INTRODUCTION

Bioactive glasses (BGs) are specialized glass biomaterials that actively interact with tissues in vivo, and unlike ordinary glass, these materials have the ability to biodegrade, increase adhesion to tissues, and promote bone growth. These abilities are controlled by the various components included in BG. In particular, the biodegradation can be finely controlled by adjusting the SiO_2 content among the components of BG, which allows for precise control of the dissolution rate. This solves the problem of low solubility of biomaterials such as hydroxyapatite, a well-known artificial bone graft material.[1−4] Unlike typical biomaterials, BGs can be further expanded in versatility by controlling and adding composition. Thus, these properties provide conditions under which they can be tailored to meet the needs of a specific medical environment or patient.[5−7] This indicates that BGs have significant potential in various fields such as bone regeneration, dental implants, tissue engineering, and medical device development.[8−11]

Discovered in the 1960s, 45S5 BG is composed of four components (SiO_2: 45 wt %, Na_2O: 24.5 wt %, CaO: 24.5 wt %, and P_2O_5: 6 wt %),[12−15] and in the 1990s, S53P4 BG (SiO_2: 53 wt %, Na_2O: 23 wt %, CaO: 20 wt %, and P_2O_5: 4 wt %) with enhanced antimicrobial properties was reported, resulting in various products such as PerioGlas, NovaBone, and BonAlive.[16−19] Among these, several studies have shown that S53P4 BG provides superior antimicrobial properties and inhibits bacterial growth in vivo compared to that of 45S5 BG.[20,21] This is because the high silica content of S53P4 BG enhances its water−glass properties, and the exchange of alkali and alkaline earth ions on the BG surface with hydrogen ions in the surrounding solution occurs more rapidly. In addition, the mechanical properties of S53P4 are predicted to be superior to those of 45S5 due to the reduced Ca and P components and increased silica content, which are the main components of hydroxyapatite with lower mechanical properties. This can often be linked to cement and ceramic applications, such as construction, where research is being carried out to increase mechanical strength through silica.[22]

Received: June 28, 2024
Revised: August 27, 2024
Accepted: October 10, 2024
Published: October 17, 2024

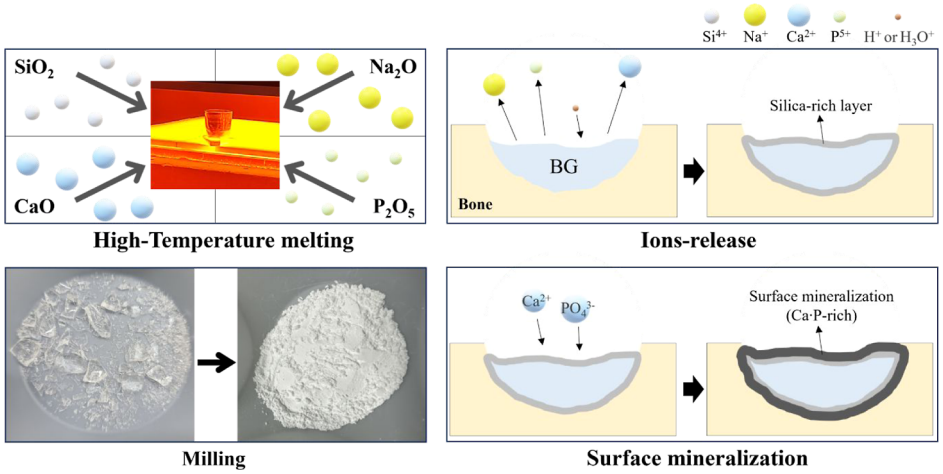

Figure 1. Schematic diagram of the preparation of S53P4 BG using the melt-milling process and the mechanism of in vitro dissolution evaluation of these BGs.

BG is currently prepared using two methods: melt-quenching and sol−gel. The melt-quenching method is a traditional and simple method in which glass precursors, such as oxides or carbonates, are mixed, homogenized, and melted at 1300−1500 °C to form glass. BG prepared through the melt-quenching method has the advantage of conferring high density and the absence of residual organic components or water. However, they come with limitations, such as challenges in mass production, a low-surface area, and being bioinert when the SiO_2 content exceeds 60 mol %.[23,24] This limitation is because BGs prepared through the melt-quenching method have a low-surface area, even with the increasing content of SiO_2. Low-surface area makes it difficult for cells to adhere and grow for bioactivity. In the sol−gel method, an aqueous solution of a precursor (alkoxide and/or metal salt) is stirred, hydrolyzed, and condensed to produce a clear sol. This solution is then dried, aged for an extended period of time, and calcined to obtain glassy granules or monolithic forms. This method offers the advantage of occurring at low temperatures, conferring a high specific surface area and nanoporosity, and being able to accommodate a wider range of SiO_2 up to 90 mol %.[25−27] In addition, these BGs have a nanosized particle size and are highly homogeneous. This provides a uniform surface area for interaction with cells and is bioactive even with a high SiO_2 content. However, currently, only silica-based BG prepared using the melt quenching method have been clinically applied and commercialized.[28,29]

BG has a chemical composition similar to that of minerals found in the body, which enhances their interaction with bone and tissue, thereby more effectively supporting the process of bone tissue formation and regeneration. In addition, the surface of BG possesses characteristics that promote cell adhesion and growth, resulting in more natural tissue regeneration.[30−33] These properties are achieved through ion release and mineralization. Ion release refers to the breakdown and absorption of a material or tissue in vivo, typically occurring simultaneously with the formation of replacement tissue. Ion release also plays an important role in the bone regeneration process, especially in the case of implants or bone regeneration, where the degradation of materials is coupled with the formation of natural bone tissue.[34] Following ion release, mineralization occurs as a process involving the creation of minerals and the formation of tissues in vivo. In vivo, mineralization is important for various biological functions, with minerals, primarily calcium and phosphorus, being produced, a phenomenon crucial for functions such as the formation of tissues such as teeth and bones.[35] Through this process, a hydroxyapatite layer is formed on the surface of BG, promoting bone formation and regeneration.[36−38]

BG's in vitro dissolution studies are of great interest because they can easily identify the prior physicochemical processes that occur to form bone in vivo. This suggests that the dissolution behavior of the material, such as ion release, precipitation, and ionic changes, that occur when BG is eluted, is very important. Therefore, the in vitro dissolution process of BG has been confirmed in many studies in various environments such as phosphate buffered saline[39] and simulated body fluid.[40,41] However, in vitro dissolution evaluation in neutral solutions such as phosphate-buffered saline and simulated body fluid is time-consuming to confirm the ability of BG. In addition, it is difficult to determine the inherent ability of BG because the phosphate buffered saline and simulated body fluid include a component (phosphate) that can react rapidly with calcium (one of the components of BG). Therefore, according to ISO 10993-14 (biological evaluation of medical devices for ceramic), two dissolution evaluation methods were proposed: tris buffer solution, a common environment for screening materials, and citric acid solution, a rapidly eluting environment.[42] This method evaluates the BG ability in a short time because there are no components in the solution that can directly react with the dissolution products of BG.

In this work, S53P4 BG was prepared through a melt-milling process and subsequently evaluated for in vitro dissolution in tris buffer solution and citric acid solution using ion release and mineralization (Figure 1). Characterization of S53P4 BG was confirmed by composition, morphology, particle size, mechanical strength, and cell viability. The mechanical strength of S53P4 BG increased with a smaller average particle size. Therefore, we performed an in vitro dissolution evaluation of S53P4 BG with a controlled particle size of 9 μm in tris buffer and citric acid solution according to ISO 10993-14. During the dissolution of S53P4 BG in tris buffer and citric acid solutions, new particles were identified that were rod-shaped but of different lengths, all of which were layered. These layers appeared thicker in tris buffer than that in citric acid solution and were identified as calcium phosphate-based compound as a

https://doi.org/10.1021/acsomega.4c06020
ACS Omega 2024, 9, 43678−43688

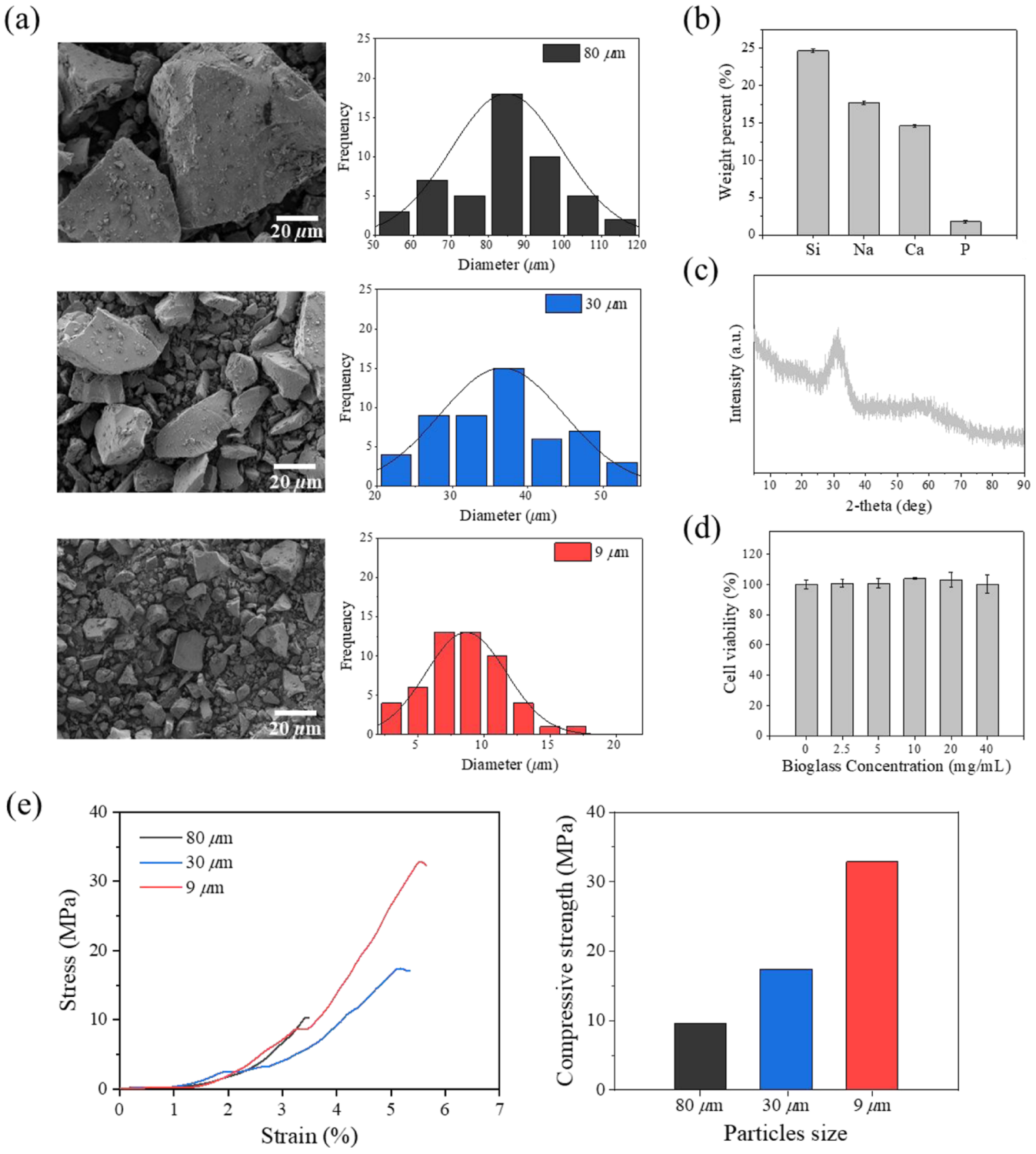

Figure 2. (a) FE-SEM images and particle size distribution of S53P4 BG at average particle sizes of 80 (top), 30 (middle), and 9 μm (bottom), (b) ICP-OES results, (c) XRD patterns, (d) cell viability results of S53P4 BG at an average particle size of 9 μm, (e) stress−strain curves and compressive strength of S53P4 BG at average particle sizes of 80, 30, and 9 μm.

result of a mineralization process. This difference was attributed to the citrate ions contained in the citric acid solution, excluding Ca ions, and we proposed a mechanism for this.

2. MATERIALS AND METHODS

2.1. Materials. Silica was purchased from Denka (Korea). Sodium carbonate, calcium carbonate, trizma base, citric acid, and sodium hydroxide were purchased from Sigma-Aldrich (USA). Sodium phosphate was purchased from Fisher Chemical. Hydrochloric acid was purchased from Daejung (Korea).

2.2. Preparation of S53P4 BG. The S53P4 BG was prepared through the melt-milling process. S53P4 BG was prepared by mixing the following powders: silica (53 wt %, 8 g), sodium carbonate (23 wt %, 5 g), calcium carbonate (20 wt %,

https://doi.org/10.1021/acsomega.4c06020
ACS Omega 2024, 9, 43678−43688

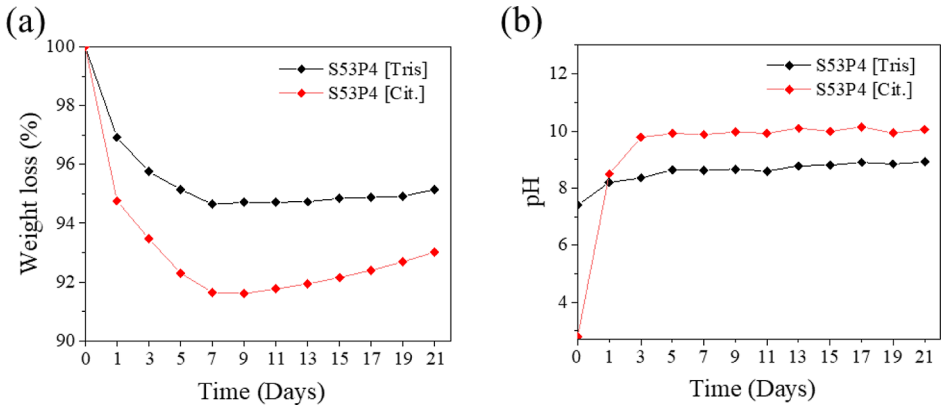

Figure 3. (a) Weight loss and (b) pH change of S53P4 BG in tris buffer and citric acid solution for 21 days.

5.5 g), and sodium phosphate (4 wt %, 1.1 g). The mixed powder of S53P4 BG was melted in a platinum crucible by heating at 600 °C for 30 min and then at 1350 °C for 2 h. The milled S53P4 BGs were homogenized using sieves of 150, 60, and 20 μm, and the milling and sieving were repeated.

2.3. Cell Viability. The S53P4 BG were sterilized with ethylene oxide gas before the experiment. The procedure involved placing S53P4 BG into the Eagle's minimum essential medium (Hyclone, USA) at different concentrations (2.5, 5, 10, 20, and 40 mg/mL) and incubating them for 24 h to obtain an extract. MG-63 cells were seeded (1×10^4 cells per well) in a 96-well plate. After 24 h, extracts of S53P4 BG at various concentrations were added to the cells. Each condition was set up in triplicate, and plates were assayed 24 h after the addition of extracts. Cell viability was assessed at 24 h using a cell counting kit (CCK-8, Dojindo). The culture medium was removed, and the samples were washed with DPBS. CCK-8 solution was added to each well (100 μL of medium and 10 μL of CCK-8 solution). Samples were incubated for 2 h at 37 °C, and supernatant (100 μL) for each sample was transferred into a nontreated 96-well plate. Absorbance at 450 nm was measured using an ELISA reader (Power wave XS; BIO-TEK).

$$\%\ \text{cell viability (absorbance: 450 nm)} = \frac{\text{mean OD}_{\text{sample}} - \text{mean OD}_{\text{blank}}}{\text{mean OD}_{\text{control}} - \text{mean OD}_{\text{blank}}} \times 100$$

2.4. Compressive Strength Evaluation. The S53P4 BG were prepared as cylindrical specimens with a diameter of 10 mm and a height of 8 mm under a pressure of 10 tons. The compressive strength of the S53P4 BG was measured using a universal mechanical testing machine (Zwick/Roell Z050) with a crosshead speed of 20 mm/min.

2.5. In Vitro Dissolution Evaluation. The in vitro dissolution evaluation of S53P4 BG was performed in accordance with ISO 10993-14 (biological evaluation of medical devices. Part 14: identification and quantification of degradation products from ceramics). The dissolution of S53P4 BG was evaluated in tris buffer and a citric acid solution. The tris buffer was prepared as follows: 13.25 g of tris(hydroxymethyl)-aminomethane was dissolved in 500 mL of distilled water and adjusted to pH 7.4 ± 1 at 37 ± 1 °C with hydrochloric acid (1 mol). The citric acid solution was prepared as follows: 21 g of citric acid powder was dissolved in 500 mL of distilled water, and 200 mL of sodium hydroxide solution was added (solution A). Then, 59.6 mL of hydrochloric acid (0.1 mol) was added to 40.4 mL of solution A and adjusted to pH to 3.0 ± 0.2 at 37 ± 1 °C. S53P4 BG (0.5 g) were added tris buffer (10 mL) and citric acid solution (10 mL), and the in vitro dissolution evaluation was performed at 37 °C for 21 days. After the dissolution evaluation in tris buffer and citric acid solution, S53P4 BG were centrifuged to separate the filtrate, washed with distilled water, and then dried in a 37 °C oven. Initial samples undergoing in vitro dissolution evaluation in tris buffer and citric acid solution for 21 days were prepared with a minimum of 9 each and were taken every 3 days to measure the weight of dried S53P4 BGs and the pH of the filtrate (including 1 day).

2.6. Instrumental Analyses. The morphology and particle sizes of S53P4 BG powder were determined by field emission scanning electron microscopy (FE-SEM) using a MIRA 3 (TESCAN, Czech) at 2 kV. The silicon, sodium, calcium, and phosphorus contents of S53P4 BG powder and the eluted filtrate were quantified by inductively coupled plasma optical emission (ICP-OES) using an Avio500 (PerkinElmer, USA). The phase of S53P4 BG powder was determined through X-ray diffraction (XRD) in the 2-theta range 3−90° using Miniflex600 (RIGAKU, Japan). The compressive strength of S53P4 BG powder was tested by a universal testing machine (UTM) using a Z050TH (Zwick Roell, Germany). The cross-section morphology and EDS analyses of S53P4 BG powder were confirmed by focused ion beam (FIB) using a Helios 5 UC (ThermoScientific, USA).

3. RESULTS AND DISCUSSION

The particle size distribution, composition ratio, X-ray pattern, cell viability, and compressive strength of S53P4 BG, using FE-SEM, ICP-OES, XRD, CCK-8 assay, and UTM are shown in Figure 2. Figure 2a shows the FE-SEM images of the S53P4 BG with respect to particle size. S53P4 BG exhibit a polygonal shape. Particle size distributions in the FE-SEM images were measured by taking 50 counts along the long axis of the particles. The average particle size for S53P4 BG was confirmed at 84.76, 36.57, and 8.6 μm, respectively. Figure 2b shows the composition ratios of S53P4 BG. The S53P4 BG composition ratios are 24.78, 17.06, 14.29, and 1.74 wt %, corresponding to Si^{4+}, Na^{+}, Ca^{2+}, and P^{5+}, respectively. These results are presented with an error range of ±1%.[6,25] Figure 2c shows the XRD patterns of the S53P4 BG. S53P4 BG exhibit an amorphous broad peak near 30 theta, characteristic of silicate glasses.[43−45] Figure 2d shows the cell viability of osteoblast-like cells (MG-63) when in contact with S53P4 BG at concentrations of 2.5, 5, 10, 20, and 40 mg/mL for 24 h. Cell viability without contact

https://doi.org/10.1021/acsomega.4c06020
ACS Omega 2024, 9, 43678−43688

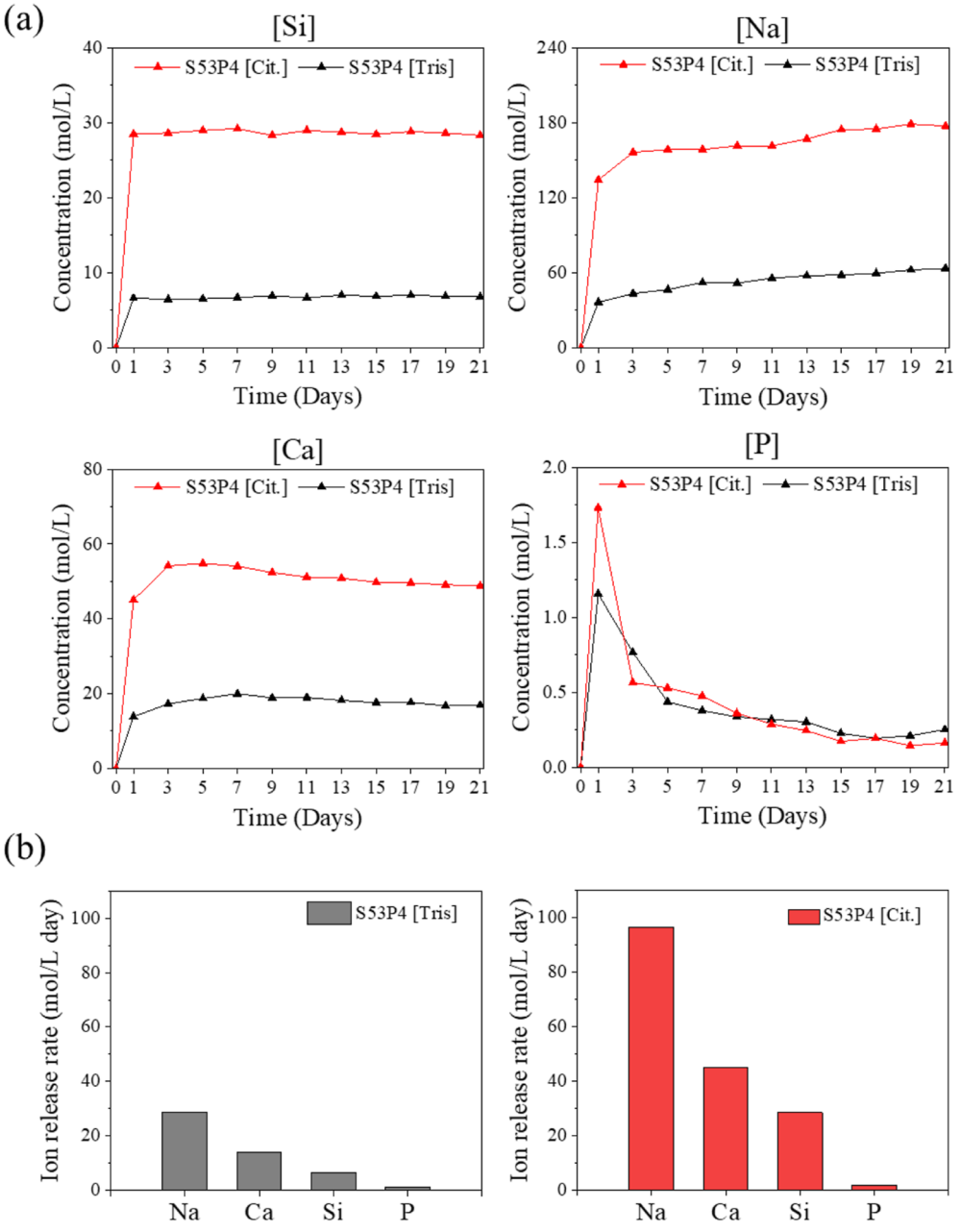

Figure 4. (a) Change in ion release concentrations of Si^{4+}, Na^{+}, Ca^{2+}, and P^{5+} from S53P4 BG in tris buffer and citric acid solutions over 21 days, and (b) ion release rates of Si^{4+}, Na^{+}, Ca^{2+}, and P^{5+} from S53P4 BG in tris buffer (left) and citric acid solution (right).

with S53P4 BG was selected as the control (shown as 0). The average particle size of the S53P4 BG used was 9 μm, with a cell viability of over 99%, indicating biocompatibility. Figure 2e shows the stress−strain curve and compressive strength of the S53P4 BG as a function of particle size. The maximum stress for S53P4 BG occurs between strains of 3.4%, 5.3%, and 5.6%, corresponding to 80, 30, and 9 μm, respectively. Also, the compressive strengths of S53P4 BG were 9.54 17.40, and 32.87 MPa. The compressive strength of S53P4 BG increases with smaller particles due to the denser internal structure resulting from the filler effect.[46] Furthermore, since materials applied in tissue regeneration typically have very low mechanical strengths, these results are very interesting because the strength can be increased with particle size. Therefore, the in vitro dissolution evaluation was performed with 9 μm S53P4 BG, which has the highest compressive strength.

Figure 3 shows the weight loss and pH change of S53P4 BG in tris buffer and citric acid solution over 21 days. As shown in Figure 3a, the weight loss of S53P4 BG is confirmed to be 4.85% in tris buffer and 6.98% in citric acid solution, respectively. The weight loss of S53P4 BG was higher in citric acid solution than that in tris buffer, attributed to the more effective dissolution of S53P4 BG in acidic citric acid solution compared to the neutral tris buffer. Furthermore, S53P4 BG in tris buffer and citric acid solution showed a decrease in weight by 7 days of the dissolution evaluation, followed by an increase by 21 days. These results predict that new particles are formed by S53P4 BG in tris buffer and citric acid solution after 7 days. Figure 3b shows the pH change of S53P4 BG in tris buffer and citric acid solution for 21 days. The pH of S53P4 BG increased from 7.4 to 8.5 in tris buffer and from 2.8 to 10 in citric acid solution over 21 days. The pH increases observed in tris buffer and citric acid solution for

https://doi.org/10.1021/acsomega.4c06020
ACS Omega 2024, 9, 43678−43688

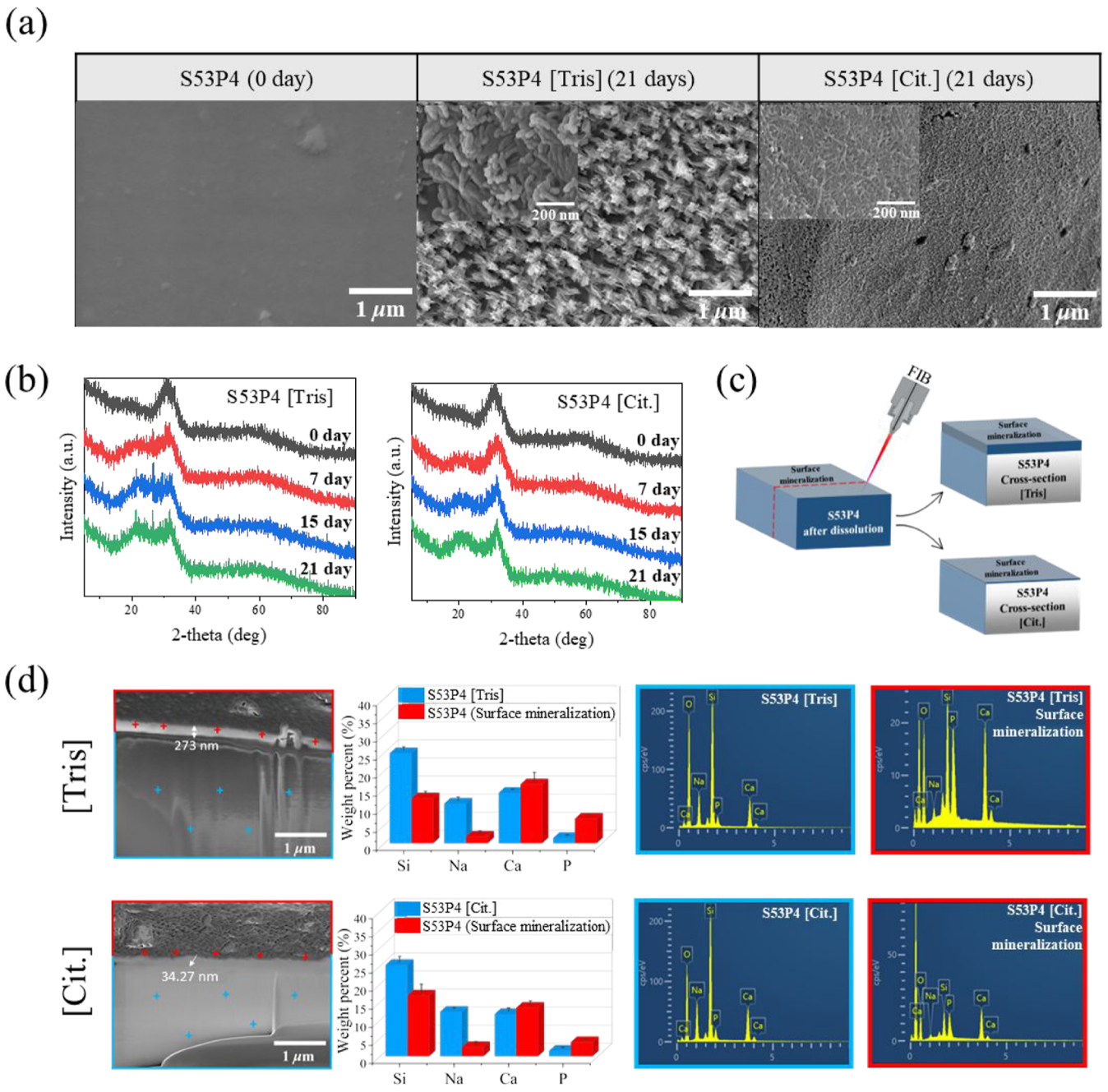

Figure 5. (a) FE-SEM images of S53P4 BG in tris buffer and citric acid solution on 0 and 21 days, (b) XRD patterns of S53P4 BG in tris buffer and citric acid solution on 0, 7, 15, and 21 days, (c) schematic of cross-sectional of S53P4 BG using FIB, and (d) FE-SEM and EDS results after cross-section of S53P4 BG after 21 days in tris buffer (top) and citric acid solution (bottom).

S53P4 BG are expected to be due to the presence of Na^+ in the BG. The influence of Na^+ on pH is explained by the rapid ion exchange of alkaline Na^+ ions with H^+ ions or H_3O^+ ions when S53P4 BG dissolve in tris buffer and citric acid solution, leading to an increase in OH^- ions during hydrolysis.

$$Si - O - Na^+ + H_2O \rightarrow Si - OH(aq) + Na^+(aq) + OH^-$$

Also, the citric acid solution exhibited a higher pH increase compared to the tris buffer. This is likely due to the faster dissolution rate in the acidic condition with a pH of 2.8, leading to a more substantial release of ions. Consequently, this increased ion release results in a more active ion exchange than that in tris buffer, leading to a higher concentration of OH^- ions and a more significant increase in pH.[47−49]

Figure 4 shows the ion release concentrations and rates of S53P4 BG in tris buffer and citric acid solution over 21 days by using ICP-OES. Figure 4a shows the Si^{4+}, Na^+, Ca^{2+}, and P^{5+} ion release concentrations of S53P4 BG in tris buffer and citric acid solution for 21 days. The Si^{4+} ion concentration of S53P4 BG on day 1 in tris buffer and citric acid solution increased rapidly to 6.58 and 28.47 mol/L, respectively, and was maintained until 21 days. The Na^+ ion concentration of S53P4 BG on day 1 in tris buffer and citric acid solution increased rapidly to 36.34 and 134.16 mol/L and continuously rising to 63.44 and 177.35 mol/L on 1−21 days, respectively. This continuous release of Na^+

https://doi.org/10.1021/acsomega.4c06020
ACS Omega 2024, 9, 43678−43688

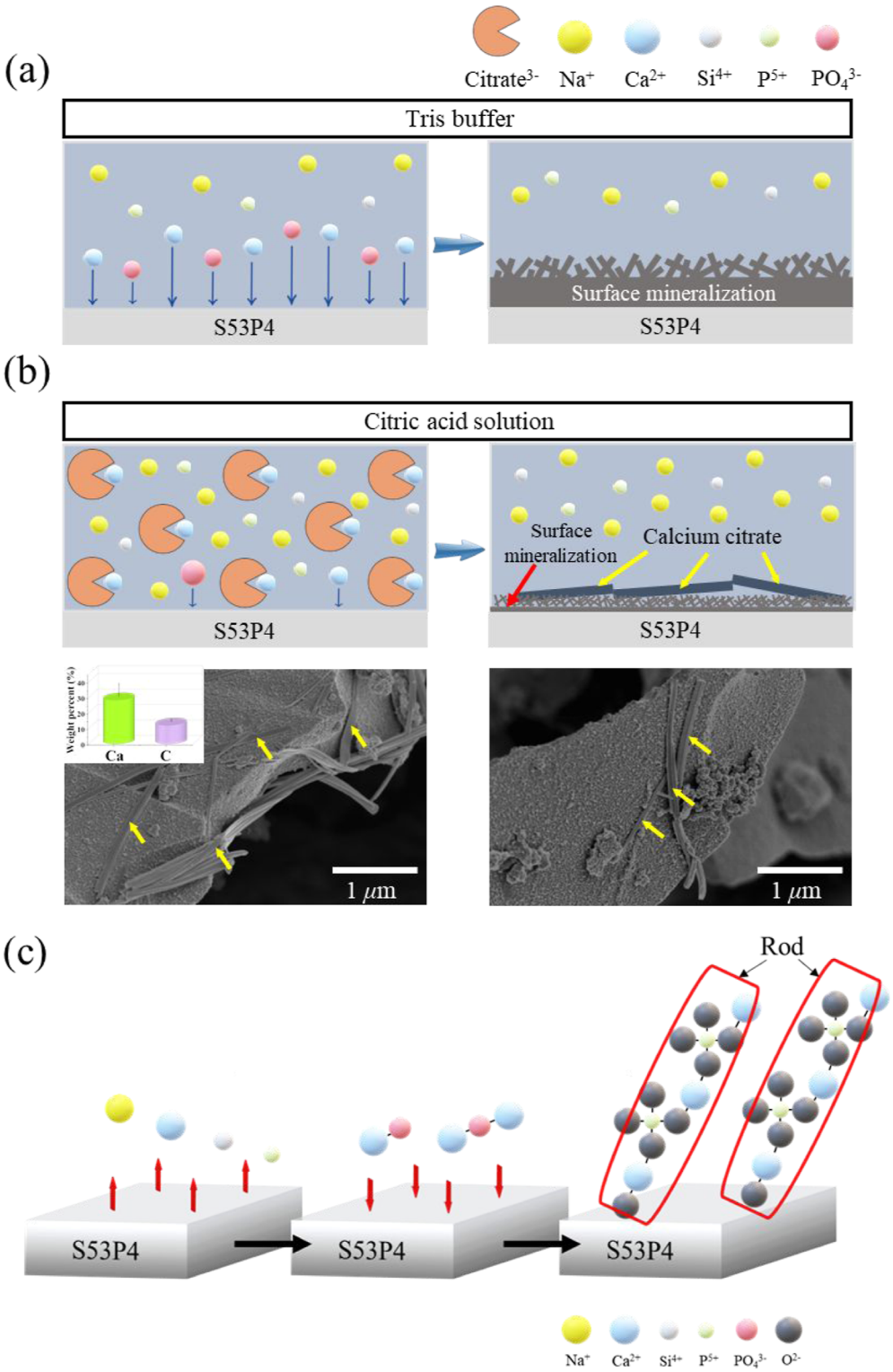

Figure 6. Schematic diagram: (a) surface mineralization of S53P4 BG in tris buffer and (b) citric acid solution, along with the FE-SEM and EDS results, and (c) process of rod-shaped calcium phosphate-based compound formation by mineralization of the S53P4 BG surface during in vitro dissolution evaluation.

ions contributes to the increase in pH in Figure 3b. In tris buffer and citric acid solution, the Ca^{2+} ion concentration of S53P4 BG increased rapidly to 17.28 and 54.12 mol/L over 3 days and then decreased continuously to 16.89 and 48.85 mol/L, respectively. In addition, the P^{5+} ion concentration in S53P4 BG increased rapidly to 1.15 and 1.73 mol/L over day 1 and then decreased continuously to 0.25 and 0.16 mol/L by 21 days, respectively. These changes in Ca^{2+} and P^{5+} ion concentrations are due to their release from the surface of S53P4 BG and their immediate reprecipitation. This is believed to be responsible for the increase in the weight of S53P4 BG, as shown in Figure 3a. In addition, Si^{4+} ions are released from the S53P4 BG, but the ion

https://doi.org/10.1021/acsomega.4c06020
ACS Omega 2024, 9, 43678−43688

concentration is maintained, which may also contribute to the weight increase. As a result, the ion release occurred more prominently in citric acid solution than that in tris buffer.[50] Figure 4b shows the ion release rate of S53P4 BG in tris buffer and citric acid solution. The ion release rates for each element in the S53P4 BG were higher in the order $Na^+ > Ca^{2+} > Si^{4+} > P^{5+}$. Moreover, S53P4 BG confirmed faster ion release rates in citric acid solution than that in tris buffer, approximately 3, 3, 5, and 1.5 times, respectively, corresponding to Na^+, Ca^{2+}, Si^{4+}, and P^{5+} ions.

$$\text{release kinetics} = \frac{\Delta[\text{release rate}]}{\Delta[\text{day}]}$$

Consequently, ion release of S53P4 BG occurred more quickly and in greater amounts in a citric acid solution than that in a tris buffer.

Figure 5 shows FE-SEM images, XRD patterns, and FIB and EDS results of S53P4 BG after in vitro dissolution evaluation in tris buffer and citric acid solution. Figure 5a shows the FE-SEM image of S53P4 BG (surface) in tris buffer and citric acid solution at 0 and 21 days. The surface morphology of the S53P4 BG on 0 day was very clean. However, the surface of S53P4 BG after 21 days was covered with newly rod-shaped particles in both tris buffer and citric acid solution. These new particles were observed as thicker and longer shaped in tris buffer but thinner in citric acid solution. They formed during the dissolution of S53P4 BG and are the result of mineralization. Mineralization involves the deposition of mineral layers in bone and tissue. Through this process, mineral-based skeletal structures, such as bone, develop and regenerate, and tissue regeneration occurs. The mineralization in the dissolution evaluation involves the precipitation of ions such as Ca^{2+} and PO_4^{3-} on the surface of S53P4 BG, leading to mineralization occurring through nucleation and growth, resulting in the formation of a calcium phosphate layer.[51] Figure 5b shows the XRD patterns of S53P4 BG in tris buffer and citric acid solution for 0, 7, 15, and 21 days. The XRD pattern of S53P4 BG confirmed only a broad peak at 30° in both tris buffer and citric acid solution at 0 day, but much broader peaks in the range of 20−30° were present at 7, 15, and 21 days. As a result, no sharp crystalline peaks were identified in the XRD pattern of S53P4 BG after 21 days, but the broad peaks at 20−30° suggest that it is a calcium phosphate-based compound when compared to previous studies.[42,52−54] Therefore, it can be expected that the layers formed on the surfaces of tris buffer and citric acid solution are composed of a calcium phosphate-based compound. Figure 5c shows a schematic diagram of the cross-section of S53P4 BG in tris buffer and citric acid solution using FIB to confirm the mineralized layers. FIB is defined as advanced equipment and techniques that use high-energy ion beams to process and image samples. FIB is primarily employed to manipulate and study matter at the nanometer and micrometer scales, with applications in semiconductor manufacturing, materials science, nanotechnology, biology, geology, and other fields.[55,56] Figure 5d shows the cross-sectional image and EDS results of S53P4 BG in tris buffer and citric acid solution. The cross-sectional morphology of S53P4 BG in tris buffer and citric acid solution was observed in two layers: below the surface of the S53P4 BG was the initial undissolved S53P4 BG layer, and above was a layer of new particles. The layer of new particles is the mineralized layer, as shown in the previous results. The thickness of the mineralized layer of S53P4 BG in tris buffer and citric acid solution was 273 and 34 nm, respectively, which means that the mineralization process is more active in tris buffer than that in citric acid solution. The EDS results of two cross-sectional layers of S53P4 BG (the initial S53P4 BG layer and the surface mineralized layer) were analyzed five times for the blue line and red line regions, respectively. The results showed that the composition ratios of the initial S53P4 BG layer in tris buffer and citric acid solution were 24.86, 10.94, 13.92, 1.44 wt % for Si, Na, Ca, and P and 25.24, 12.28, 11.64, 1.48 wt % for Si, Na, Ca, and P, respectively. The surface mineralization layers of S53P4 BG were 12.40, 1.80, 16.30, 6.80, 16.78, 2.54, 13.41, and 3.90 wt %, respectively. In other words, the surface mineralized layer in both tris buffer and citric acid solution had higher Ca and P elemental contents than the initial S53P4 BG layer. In addition, the Ca/P molar ratio of the surface mineralization layer was 1.85 and 2.66 in tris buffer and citric acid solution, respectively. Thus, the surface mineral layer of S53P4 BG is composed of calcium phosphate-based compound, and tris buffer is closer to calcium phosphate than citric acid solution.

Figure 6 shows a schematic diagram of the mineralization process and results occurring on the surface of S53P4 BG in tris buffer and citric acid solution through ion release during the in vitro dissolution evaluation. Figure 6a shows a schematic diagram of the surface mineralization process of the S53P4 BG in tris buffer. Upon dissolution evaluation in tris buffer, Na^+, Ca^{2+}, and PO_4^{3-} ions are released from the surface of the S53P4 BG. Among the released ions, Na^+ increases the pH of the solution. Also, Ca^{2+} and PO_4^{3-} react with each other when they are in the ionic state, so they precipitate and form a mineralized layer. Therefore, the longer the dissolution time, the more ions are released from S53P4 BG, and the thicker the mineralized layer. Figure 6b shows a schematic diagram of the surface mineralization process of S53P4 BG in citric acid solution with SEM images and EDS results for another new particle formed during the process. Upon dissolution evaluation of S53P4 BG in citric acid solution, similar to tris buffer, Na^+, Ca^{2+}, and PO_4^{3-} ions are released from the surface. However, these ions are released faster and in larger amounts than that in tris buffer due to the slightly acidic nature of the citric acid solution. Therefore, the pH increase over the same time period is higher in the citric acid solution than that in the tris buffer. Also, the mineralization layer precipitated by Ca^{2+} and PO_4^{3-} ions should be much thicker. However, the mineralization layer in citric acid solution was thinner than that in tris buffer. Moreover, another new rod-shaped particle was observed on the surface of S53P4 BG by SEM. This particle had a thickness of 60 nm and a length of 2 μm, and it was formed only in citric acid solution. The EDS results of this particle showed that the Ca and C elemental contents were 28.23 and 11.93 wt %, respectively. This means that this particle was formed by the citrate ions present in the citric acid solution. S53P4 BG in tris buffer formed a thick mineralization layer due to the sequential precipitation of Ca^{2+} and PO_4^{3-} ions without any interference due to the absence of citrate. However, S53P4 BG in citric acid solution contains citrate ions, which act as a scavenger of Ca^{2+} ions.[57] The chemical structure of these citrate ions has three carboxyl groups, making citrate a more active site than the PO_4^{3-} ion, predominantly reacting with Ca^{2+} ions.[58] As a result, S53P4 BG in a citric acid solution formed new rod-shaped calcium citrate particles. Thus, citrate ions bind with Ca^{2+} ions released from S53P4 BG to form calcium citrate particles, which consume most of the released Ca^{2+} ions.[59] The surface mineralization layer of S53P4 BG is then formed with a thin thickness due to the lack of Ca^{2+} ions. Therefore, calcium phosphate-based

https://doi.org/10.1021/acsomega.4c06020
ACS Omega 2024, 9, 43678−43688

compound and calcium citrate are present on the surface of S53P4 BG eluted from the citric acid solution. Figure 6c shows a schematic diagram of the process and chemical structure of rod-shaped calcium phosphate-based compound formation by mineralization on the S53P4 BG surface during in vitro dissolution evaluation. During the in vitro dissolution evaluation, various ions are released from S53P4 BG, among which Ca^{2+} and PO_4^{3-} ions interact and precipitate on the surface of S53P4 BG. The particles formed by precipitation are calcium phosphate-based compound, which undergo nucleation and nucleation growth by the continuously released Ca^{2+} and PO_4^{3-} ions depending on the elution time.[60−63] The resulting rod-shaped particles can be composed of Ca and P, forming a layer on the surface of the S53P4 BG.

Figure 7 shows the ion release and surface mineralization behavior of S53P4 BG in tris buffer and a citric acid solution.

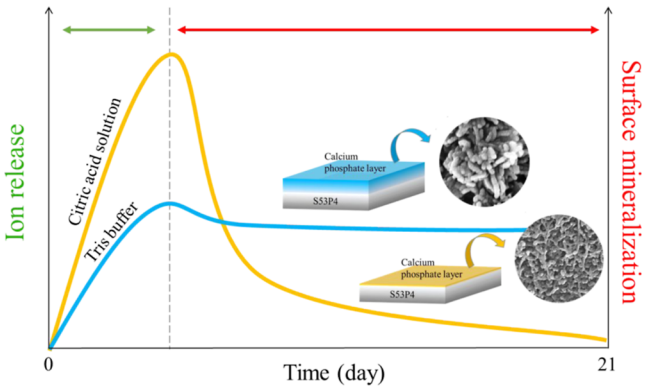

Figure 7. Schematic diagram of ion release and surface mineralization behavior of S53P4 BG in tris buffer and citric acid solution.

S53P4 BG was eluted in tris buffer and citric acid solution, ion release occurred more rapidly in citric acid solution than that in tris buffer. The ion released were then consumed by the surface mineralization process and reduced. The reduction in ion released during this process was greater in citric acid solution than that in tris buffer. Therefore, surface mineralization of S53P4 BG should occur more in citric acid solution. However, the surface mineralization of S53P4 BG occurred more in the tris buffer than that in the citric acid solution, and the mineralized particles formed in the tris buffer were thicker and longer than that in the citric acid solution. This is because the citrate ions present in the citric acid solution removed the ion released from S53P4 BG. As a result, the mineralized layer formed on the surface of S53P4 BG was nine times thicker in the tris buffer than that in the citric acid solution.

4. CONCLUSIONS

S53P4 BG prepared through the melt-milling process achieved the highest mechanical strength at an average particle size of 9 μm, and the mechanical strength decreased with an increasing average particle size. During the dissolution process, the concentration of ion released from S53P4 BG was higher in citric acid solution than that in tris buffer because the acidic solution quickly destroyed the surface of S53P4 BG. However, the mineralization of S53P4 BG occurred more actively in tris buffer than that in citric acid solution. In addition, the S53P4 BG mineralized particles observed in tris buffer had a thicker rodlike morphology than that in citric acid solution. This layer of S53P4 BG mineralized particles was identified as calcium phosphate-based compound. These results were attributed to the citrate ions present in the citric acid solution removing the Ca ion released from S53P4 BG. This was evidenced by the observation of another rodlike morphology, calcium citrate, in the citric acid solution.

AUTHOR INFORMATION

Corresponding Author

Jeong Ho Chang − *Korea Institute of Ceramic Engineering and Technology, Jinju 52851, Republic of Korea;* orcid.org/0000-0002-8222-4176; Phone: +82 43 913 1510; Email: jhchang@kicet.re.kr

Authors

Kwon Jun Yoo − *Korea Institute of Ceramic Engineering and Technology, Jinju 52851, Republic of Korea*

Woo Young Jang − *Korea Institute of Ceramic Engineering and Technology, Jinju 52851, Republic of Korea*

Complete contact information is available at: https://pubs.acs.org/10.1021/acsomega.4c06020

Author Contributions

†K.J.Y. and W.Y.J. contributed equally to this work. J.H.C.: investigation, conceptualization, review and editing, supervision, and funding acquisition. K.J.Y.: investigation and writing—original draft. W.Y.J.: investigation and editing—original draft.

Notes

The authors declare no competing financial interest.

ACKNOWLEDGMENTS

This work was supported by a grant from the R&D program funded by the Ministry of Trade, Industry and Energy (MOTIE), part of the Industry Core Technology Development Program funded by the Korea Evaluation Institute of Industrial Technology (KEIT) [20018324], Republic of Korea.

REFERENCES

(1) Rabiee, S. M.; Nazparvar, N.; Azizian, M.; Vashaee, D.; Tayebi, L. Effect of ion substitution on properties of bioactive glasses: A review. *Ceram. Int.* **2015**, *41* (6), 7241−7251.

(2) Kaur, G.; Pandey, O. P.; Singh, K.; Homa, D.; Scott, B.; Pickrell, G. A review of bioactive glasses: their structure, properties, fabrication and apatite formation. *J. Biomed. Mater. Res., Part A* **2014**, *102* (1), 254−274.

(3) Fernandes, H. R.; Gaddam, A.; Rebelo, A.; Brazete, D.; Stan, G. E.; Ferreira, J. M. Bioactive glasses and glass-ceramics for healthcare applications in bone regeneration and tissue engineering. *Materials* **2018**, *11* (12), 2530.

(4) Jones, J. R.; Brauer, D. S.; Hupa, L.; Greenspan, D. C. Bioglass and bioactive glasses and their impact on healthcare. *Int. J. Appl. Glass Sci.* **2016**, *7* (4), 423−434.

(5) Fandzloch, M.; Bodylska, W.; Augustyniak, A. W.; Roszek, K.; Jaromin, A.; Lukowiak, A. Bioactive nanoglasses and xerogels (SiO_2−CaO and SiO_2−CaO−P_2O_5) as promising candidates for biomedical applications. *Ceram. Int.* **2023**, *49* (5), 7438−7451.

(6) Azzouz, I.; Khlifi, K.; Faure, J.; Dhiflaoui, H.; Larbi, A. B. C.; Benhayoune, H. Mechanical behavior and corrosion resistance of sol-gel derived 45S5 bioactive glass coating on Ti6Al4V synthesized by electrophoretic deposition. *J. Mech. Behav. Biomed. Mater.* **2022**, *134*, 105352.

(7) Workie, A. B.; Shih, S.-J. A study of bioactive glass−ceramic's mechanical properties, apatite formation, and medical applications. *RSC Adv.* **2022**, *12* (36), 23143−23152.

(8) Shearer, A.; Montazerian, M.; Sly, J. J.; Hill, R. G.; Mauro, J. C. Trends and perspectives on the commercialization of bioactive glasses. *Acta Biomater.* **2023**, *160*, 14−31.
(9) Negut, I.; Ristoscu, C. Bioactive glasses for soft and hard tissue healing applications—A short review. *Appl. Sci.* **2023**, *13* (10), 6151.
(10) Ege, D.; Zheng, K.; Boccaccini, A. R. Borate bioactive glasses (BBG): bone regeneration, wound healing applications, and future directions. *J. Appl. Biomater.* **2022**, *5* (8), 3608−3622.
(11) Jafari, N.; Habashi, M. S.; Hashemi, A.; Shirazi, R.; Tanideh, N.; Tamadon, A. Application of bioactive glasses in various dental fields. *Biomater. Res.* **2022**, *26* (1), 31.
(12) Jones, J. R. Review of bioactive glass: from Hench to hybrids. *Acta Biomater.* **2013**, *9* (1), 4457−4486.
(13) Hench, L. L. The story of Bioglass. *J. Mater. Sci.: Mater. Med.* **2006**, *17* (11), 967−978.
(14) Fu, H.; Rahaman, M. N.; Day, D. E.; Huang, W. Long-term conversion of 45S5 bioactive glass−ceramic microspheres in aqueous phosphate solution. *J. Mater. Sci.: Mater. Med.* **2012**, *23*, 1181−1191.
(15) Rizwan, M.; Hamdi, M.; Basirun, W. J. Bioglass® 45S5-based composites for bone tissue engineering and functional applications. *J. Biomed. Mater. Res., Part A* **2017**, *105* (11), 3197−3223.
(16) Kermani, F.; Vojdani-Saghir, A.; Beidokhti, S. M.; Nazarnezhad, S.; Mollaei, Z.; Hamzehlou, S.; El-Fiqi, A.; Baino, F.; Kargozar, S. Iron (Fe)-doped mesoporous 45S5 bioactive glasses: Implications for cancer therapy. *Transl. Oncol.* **2022**, *20*, 101397.
(17) Kermani, F.; Nazarnezhad, S.; Mollaei, Z.; Mollazadeh, S.; Ebrahimzadeh-Bideskan, A.; Askari, V. R.; Oskuee, R. K.; Moradi, A.; Hosseini, S. A.; Azari, Z.; et al. Zinc-and copper-doped mesoporous borate bioactive glasses: Promising additives for potential use in skin wound healing applications. *Int. J. Mol. Sci.* **2023**, *24* (2), 1304.
(18) Yang, S.-Y.; Kim, S.-H.; Choi, S.-Y.; Kim, K.-M. Acid neutralizing ability and shear bond strength using orthodontic adhesives containing three different types of bioactive glass. *Materials* **2016**, *9* (3), 125.
(19) Andersson, Ö. H.; Liu, G.; Karlsson, K. H.; Niemi, L.; Miettinen, J.; Juhanoja, J. In vivo behaviour of glasses in the SiO_2-Na_2O-CaO-P_2O_5-Al_2O_3-B_2O_3 system. *J. Mater. Sci.: Mater. Med.* **1990**, *1*, 219−227.
(20) Andersson, Ö. H.; Kangasniemi, I. Calcium phosphate formation at the surface of bioactive glass in vitro. *J. Biomed. Mater. Res.* **1991**, *25* (8), 1019−1030.
(21) Fagerlund, S.; Hupa, L.; Hupa, M. Dissolution patterns of biocompatible glasses in 2-amino-2-hydroxymethyl-propane-1, 3-diol (Tris) buffer. *Acta Biomater.* **2013**, *9* (2), 5400−5410.
(22) Li, B.; Gao, A.; Li, Y.; Xiao, H.; Chen, N.; Xia, D.; Wang, S.; Li, C. Effect of silica fume content on the mechanical strengths, compressive stress−strain behavior and microstructures of geopolymeric recycled aggregate concrete. *Constr. Build. Mater.* **2023**, *384*, 131417.
(23) Barros, A. A.; Leite, A. J.; Pires, R. A.; Mano, J. F.; Reis, R. L. Bioactive Composites Reinforced with Inorganic Glasses and Glass−Ceramics for Tissue Engineering Applications. In *Advances in Calcium Phosphate Biomaterials*; Springer Berlin Heidelberg, 2014; pp 331−353.
(24) Wood, D.; Hill, R. Glass ceramic approach to controlling the properties of a glass-ionomer bone cement. *Biomater* **1991**, *12* (2), 164−170.
(25) Fiume, E.; Migneco, C.; Verné, E.; Baino, F. Comparison between bioactive sol-gel and melt-derived glasses/glass-ceramics based on the multicomponent SiO_2−P_2O_5−CaO−MgO−Na_2O−K_2O system. *Materials* **2020**, *13* (3), 540.
(26) Ben-Arfa, B. A.; Pullar, R. C. A comparison of bioactive glass scaffolds fabricated by robocasting from powders made by sol−gel and melt-quenching methods. *Processes* **2020**, *8* (5), 615.
(27) Palakurthy, S.; Azeem, P. A.; Reddy, K. V. Sol−gel synthesis of soda lime silica-based bioceramics using biomass as renewable sources. *J. Korean Ceram. Soc.* **2022**, *59* (1), 76−85.
(28) Hupa, L.; Wang, X.; Eqtesadi, S. Bioactive Glasses. In *Springer Handbook of Glass*; Musgraves, J. D., Hu, J., Calvez, L., Eds.; Springer International Publishing, 2019; pp 813−849.
(29) Arcos, D.; Vallet-Regí, M. Sol−gel silica-based biomaterials and bone tissue regeneration. *Acta Biomater.* **2010**, *6* (8), 2874−2888.
(30) Zheng, K.; Niu, W.; Lei, B.; Boccaccini, A. R. Immunomodulatory bioactive glasses for tissue regeneration. *Acta Biomater.* **2021**, *133*, 168−186.
(31) Cannillo, V.; Salvatori, R.; Bergamini, S.; Bellucci, D.; Bertoldi, C. Bioactive glasses in periodontal regeneration: existing strategies and future prospects—a literature review. *Materials* **2022**, *15* (6), 2194.
(32) Vallet-Regi, M.; Salinas, A. J. Mesoporous bioactive glasses for regenerative medicine. *Mater. Today Bio* **2021**, *11*, 100121.
(33) Abushahba, F.; Algahawi, A.; Areid, N.; Hupa, L.; Närhi, T. O. Bioactive glasses in periodontal regeneration: a systematic review. *Tissue Eng., Part C* **2023**, *29* (5), 183−196.
(34) Jaturapitakkul, C.; Tangpagasit, J.; Songmue, S.; Kiattikomol, K. Filler effect of fine particle sand on the compressive strength of mortar. *Int. J. Miner., Metall. Mater.* **2011**, *18* (2), 240−246.
(35) Boskey, A. L. Biomineralization: an overview. *Connect. Tissue Res.* **2003**, *44* (1), 5−9.
(36) Jablonská, E.; Horkavcová, D.; Rohanová, D.; Brauer, D. S. A review of in vitro cell culture testing methods for bioactive glasses and other biomaterials for hard tissue regeneration. *J. Mater. Chem. B* **2020**, *8* (48), 10941−10953.
(37) Kargozar, S.; Mozafari, M.; Ghenaatgar-Kasbi, M.; Baino, F. Bioactive glasses and glass/polymer composites for neuroregeneration: should we be hopeful? *Appl. Sci.* **2020**, *10* (10), 3421.
(38) Jiménez-Holguín, J.; Arcos, D.; Lozano, D.; Saiz-Pardo, M.; de Pablo, D.; Ortega, L.; Enciso, S.; Fernández-Tomé, B.; Díaz-Güemes, I.; Sánchez-Margallo, F. M.; et al. In vitro and in vivo response of zinc-containing mesoporous bioactive glasses in a sheep animal model. *Int. J. Mol. Sci.* **2022**, *23* (22), 13918.
(39) Yusof, N. N.; Aziz, S. M.; Noor, F. M.; Yaacob, S. N. S.; Hashim, S. A novel borate-based 45S5 Bioglass®: In vitro assessment in phosphate-buffered saline solution. *J. Non-Cryst. Solids* **2022**, *596*, 121843.
(40) Hench, L. L. Bioceramics: from concept to clinic. *J. Am. Ceram. Soc.* **1991**, *74* (7), 1487−1510.
(41) Souza, L.; Lopes, J. H.; Encarnação, D.; Mazali, I. O.; Martin, R. A.; Camilli, J. A.; Bertran, C. A. Comprehensive in vitro and in vivo studies of novel melt-derived Nb-substituted 45S5 bioglass reveal its enhanced bioactive properties for bone healing. *Sci. Rep.* **2018**, *8* (1), 12808.
(42) ISO 10993-14. *Biological Evaluation of Medical Devices, Part 14: Identification And Quantification of Degradation Products From Ceramics*; International Standard, 2001.
(43) Hench, L. L.; Wilson, J. Surface-active biomaterials. *Science* **1984**, *226* (4675), 630−636.
(44) Bretcanu, O.; Chatzistavrou, X.; Paraskevopoulos, K.; Conradt, R.; Thompson, I.; Boccaccini, A. R. Sintering and crystallisation of 45S5 Bioglass® powder. *J. Eur. Ceram. Soc.* **2009**, *29* (16), 3299−3306.
(45) Mačković, M.; Hoppe, A.; Detsch, R.; Mohn, D.; Stark, W. J.; Spiecker, E.; Boccaccini, A. R. Bioactive glass (type 45S5) nanoparticles: in vitro reactivity on nanoscale and biocompatibility. *J. Nanopart. Res.* **2012**, *14*, 966.
(46) Aalto-Setälä, L.; Uppstu, P.; Sinitsyna, P.; Lindfors, N. C.; Hupa, L. Dissolution of amorphous S53P4 glass scaffolds in dynamic in vitro conditions. *Materials* **2021**, *14* (17), 4834.
(47) Lee, S. W.; Park, O.; Kang, S.; Rho, H. T.; Kim, S.-I. Physicochemical characteristics of mineral trioxide aggregate depending on the ratio of di-and tricalcium silicates. *J. Korean Ceram. Soc.* **2023**, *60* (6), 1028−1035.
(48) Fiume, E.; Barberi, J.; Verné, E.; Baino, F. Bioactive glasses: from parent 45S5 composition to scaffold-assisted tissue-healing therapies. *J. Funct. Biomater.* **2018**, *9* (1), 24.
(49) Vasconcelos, E. V.; da Luz, F. B.; da Paz, S. P. A.; dos Reis, M. A. L.; da Silva, A. C. R.; Passos, M. F.; Barboza, C. A. G.; Monteiro, S. N.; Candido, V. S. Nanostructured 3D bioprinting of PLA with bioglass-CNT scaffolds for osseus tissue graft manufacturing. *J. Mater. Res. Technol.* **2023**, *23*, 5923−5938.
(50) Sprio, S.; Antoniac, I.; Chevalier, J.; Iafisco, M.; Sandri, M.; Tampieri, A. Editorial: Recent advances in bioceramics for health. *Front. Bioeng. Biotechnol.* **2023**, *11*..

https://doi.org/10.1021/acsomega.4c06020
ACS Omega 2024, 9, 43678−43688

(51) Liu, C.; Cui, X.; Du, Y.; Wang, X.; Kim, J.; Li, S.; Zhang, L.; Zhao, X.; Zhao, L.; Tian, P.; et al. Unusual Surface Coagulation Activation Patterns of Crystalline and Amorphous Silicate-Based Biominerals. *Adv. Healthcare Mater.* **2023**, *12* (20), 2300039.
(52) Rohanová, D.; Boccaccini, A. R.; Yunos, D. M.; Horkavcová, D.; Březovská, I.; Helebrant, A. TRIS buffer in simulated body fluid distorts the assessment of glass−ceramic scaffold bioactivity. *Acta Biomater.* **2011**, *7* (6), 2623−2630.
(53) Sinitsyna, P.; Karlström, O.; Sevonius, C.; Hupa, L. In vitro dissolution and characterisation of flame-sprayed bioactive glass microspheres S53P4 and 13−93. *J. Non-Cryst. Solids* **2022**, *591*, 121736.
(54) Mozafari, M.; Banijamali, S.; Baino, F.; Kargozar, S.; Hill, R. G. Calcium carbonate: Adored and ignored in bioactivity assessment. *Acta Biomater.* **2019**, *91*, 35−47.
(55) Tseng, A. A. Recent developments in nanofabrication using focused ion beams. *Small* **2005**, *1* (10), 924−939.
(56) Bassim, N.; Scott, K.; Giannuzzi, L. A. Recent advances in focused ion beam technology and applications. *MRS Bull.* **2014**, *39* (4), 317−325.
(57) Mitsionis, A. I.; Vaimakis, T. C.; Trapalis, C. C. The effect of citric acid on the sintering of calcium phosphate bioceramics. *Ceram. Int.* **2010**, *36* (2), 623−634.
(58) Pooresmaeil, M.; Javanbakht, S.; Namazi, H.; Shaabani, A. Application or function of citric acid in drug delivery platforms. *Med. Res. Rev.* **2022**, *42* (2), 800−849.
(59) Liu, X.-C.; Skibsted, L. H. Citrate in calcium transport and biomineralisation. *Int. Dairy J.* **2023**, *139*, 105561.
(60) Eliaz, N.; Metoki, N. Calcium phosphate bioceramics: a review of their history, structure, properties, coating technologies and biomedical applications. *Materials* **2017**, *10* (4), 334.
(61) Lin, K.; Wu, C.; Chang, J. Advances in synthesis of calcium phosphate crystals with controlled size and shape. *Acta Biomater.* **2014**, *10* (10), 4071−4102.
(62) Jang, W. Y.; Pyun, J. C.; Chang, J. H. Comparative In Vitro Dissolution Assessment of Calcined and Uncalcined Hydroxyapatite Using Differences in Bioresorbability and Biomineralization. *Int. J. Mol. Sci.* **2024**, *25* (1), 621.
(63) Sunarso; Rino; Qalbina, T.; Indrani, D. J.; Herda, E.; Pangesty, A. I. Effect of hydrothermal temperature on phase transformation and mechanical property of non-sintered hydroxyapatite and its in vitro solubility. *J. Korean Ceram. Soc.* **2023**, *60* (1), 215−223.

https://doi.org/10.1021/acsomega.4c06020
ACS Omega 2024, 9, 43678−43688